Microring Circulator Embedded Plasmonic Island for Multi-probe Bio-cell Sensors

IOP Conf. Series: Materials Science and Engineering **536** (2019) 012009 doi:10.1088/1757-899X/536/1/012009

Microring Circulator Embedded Plasmonic Island for Multi-probe Bio-cell Sensors

N. Pornsuwanchaoren[1], P. Youplao[1], K. Chaiwong[2], I.S. Amiri[3], J. Ali[4], P. Yupapin [5, 6*]

[1]Department of Electrical Engineering, Faculty of Industry and Technology, Rajamangala University of Technology Isan, Sakon Nakhon Campus, 199 Phungkon, Sakon Nakhon 47160, Thailand;
[2]Department of Electrical and Electronics Engineering, Faculty of Industrial Technology, Loei Rajabhat University, Loei, 42000, Thailand;
[3]Division of Materials Science and Engineering, Boston University, Boston, MA, 02215, USA;
[4]Laser Centre, IBNU SINA ISIR, Universiti Teknologi Malaysia 81310 Johor Bahru, Malaysia;
[5]Computational Optics Research Group, Advanced Institute of Materials Science, Ton Duc Thang University, District 7, Ho Chi Minh City, Vietnam;
[6]Faculty of Applied Sciences, Ton Duc Thang University, District 7, Ho Chi Minh City, Vietnam;

*E-mail: preecha.yupapin@tdtu.edu.vn

Abstract: Three different wavelength light sources are coupled to microring circulator via modified add-drop multiplexers, from which the multiplexed signals of them can be formed at the plasmonic islands and used as the distributed sensor nodes. The change in the wavelength due to the external environment will affect the refractive index of the sensing material and hence shift in each wavelength will be seen. Measurements are recorded as the shift in a spectrum ($\Delta\lambda$) by changing the input power and a relationship is obtained between the change in input power and shift in the output spectrum for 1.10, 1.30 and 1.55 μm wavelengths. This is the micro-scale device that can be used for bio-cell content distributed sensors, in which the three different aspects of sensor mechanism can be employed.

Keywords: Distributed sensors; Multiplexed sensors; Optical sensors; Optical circulator; Microring sensor;

1. Introduction

The plasmonic island has become a promising electro-optic device that can be made to use electrical and optical signals for taking measurements. Recently, there are several articles published which report very interesting aspects of these devices [1-4], in which the conversion between the electrical and optical signals are shown to be obtained through stacked layers of silicon-graphene-gold materials, which is known as a plasmonic island [5]. Another advantage is that the conversion of the signals can be functioned within the center of the system, where the energy is supplied by the whispering gallery mode(WGM) of light generated within a microring resonator. It is a nonlinear microring device, in which the WGM can be controlled by the two nonlinear side rings [6-9]. Experimental evidence of the WGM generated by the ring resonator have been confirmed with a wide range of applications [10, 11], which gives us more confidence in the realistic application of our proposed device. Up to date, various works have been theoretically proposed with potential

applications [12-14], where most of them use the microring resonator structure known as a panda-ring resonator. In this article, we have proposed the use of the optical circulator of three light sources for cross-connection, which is available for the multi-wavelength multiplexing and is useful for LiFi link and for high traffic data communication. One more interesting application is that the circulation nodes, which are constructed by the panda-ring resonator, can be employed as sensor nodes of the distributed sensors, in which large area detection can be performed. The electro-optic signal conversion can also performed, which enables the employability of distributed sensors in both electrical and light signal applications. By using the stacked layers of silicon-graphene-gold called the plasmonic island [6], the conversion of light and the electrical signal can be achieved. The proposed system is schematically illustrated in Figure 1. Equations (1)-(3) represent the electrical output fields of the circuit [15]. The WGM field ($\mathbf{E_{WGM}}$) is given in the cylindrical coordinates [16]. To simplify the equation, the surface reflection of the reflector is neglected, where $\mathbf{I_{WGMR}} = -\mathbf{R_{WGM}}\ \mathbf{I_{WGMR}}.\ \mathbf{R_{WGM}}$ which is the reflection output. In the case of multi-input and output (MIMO) signal applications, the three-wavelength input sources to the system and cross-connected source wavelengths are used to form the simultaneous multi-wavelength sensors, where the sensor heads are at the WGM outputs of each node. The distributed sensors are formed by the large area of the sensors and can perform simultaneous measurements. The used parameters are given in the captions of relevant figures.

2. Theoretical Background

The sensor system is shown in Figure 1. Three selected light sources are fed into the system via the input ports. The input port field is represented by the input electric field ($\boldsymbol{E_{in}}$) of each input with the different wavelengths. The electric fields are circulated within the system and the sensor nodes(islands). The input electric field is fed into the z-axis, which is given by $\boldsymbol{E_{in}} = \boldsymbol{E_Z} = \boldsymbol{E_0 e^{-ik_z-\omega t+\varphi}}$, $\boldsymbol{E_0}$ is the initial electric field amplitude, where $\boldsymbol{E_0}$ is the electric field amplitude (real), $\boldsymbol{k_z} = 2\pi/\lambda_i$ is the wave number in the direction of propagation (z-axis), i=1, 2, 3. $\boldsymbol{\omega}$ and φ are the angular frequency and $phase\ of\ light$ associated with the input light source wavelengths. The distributed electrical fields within the system are given as the following details. For simplicity, three light sources are simultaneously fed into the system, in which the distance from the source to the coupling node is kept the same. The output signals of the through(E_{th}), drop(E_{dr}) and add(E_{add}) ports can be expressed as explained by J. Ali et al.[17].

$$\boldsymbol{E_{th_1}} = \left[\frac{\boldsymbol{G.F^2 - G.F.C - A.H.J}}{\boldsymbol{F^2.J - C.F.J}}\right]\boldsymbol{E_{in_1}} + \left[\frac{\boldsymbol{(F.I - B.H - C.I)}}{\boldsymbol{F.(F-C)}}\right]\boldsymbol{E_{ad_1}} \quad (1)$$

$$\boldsymbol{E_{dr_1}} = \frac{\boldsymbol{K(F-C-BL/K)E_{ad_1} - L.A.E_{in_1}}}{\boldsymbol{M(F-C)}} \quad (2)$$

$$\boldsymbol{E_{ad_1}} = \boldsymbol{E_{dr_5}}(\sqrt{\mathbf{1-\kappa}} - \sqrt{\boldsymbol{\kappa}}^2(\frac{\boldsymbol{S}}{\boldsymbol{S-T}}) \quad (3)$$

where the parameters of nodes 1, 3, 5 are given by

$$\mathbf{A} = (x_1z_1PL_8 - x_1z_1x_2y_2P_1PL_8 - x_1z_1x_4y_4P_2PL_8 + x_1z_1x_2y_2x_4y_4P_1P_2PL_8)$$

$$\begin{aligned}\boldsymbol{B} = (&x_1y_1x_3z_3x_4y_4PL_4PL_8 - x_1y_1x_2y_2x_3z_3x_4y_4P_1PL_4PL_8 - x_1y_1x_3z_3x_4^2y_4^2P_2PL_4PL_8\\ &+ x_1y_1x_2y_2x_3z_3x_4^2y_4^2P_1P_2PL_8PL_4 - x_1y_1x_3z_3x_4^2z_4^2P_2PL_4PL_8\\ &+ x_1y_1x_2y_2x_3z_3x_4^2z_4^2P_1P_2PL_4PL_8)\end{aligned}$$

$$\begin{aligned}\boldsymbol{C} = \ [&x_1y_1x_2y_2x_3y_3x_4y_4(PL_4)^2 - x_1y_1x_2^2y_2^2x_3y_3x_4y_4P_1(PL_4)^2 - x_1y_1x_2^2z_2^2x_3y_3x_4y_4P_1(PL_4)^2\\ &- x_1y_1x_2y_2x_3y_3x_4^2y_4^2P_2(PL_4)^2 + x_1y_1x_2^2y_2^2x_3y_3x_4^2y_4^2P_1P_2(PL_4)^2\\ &+ x_1y_1x_2^2z_2^2x_3y_3x_4^2y_4^2P_1P_2(PL_4)^2 - x_1y_1x_2y_2x_3y_3x_4^2z_4^2P_2(PL_4)^2\\ &+ x_1y_1x_2^2y_2^2x_3y_3x_4^2z_4^2P_1P_2(PL_4)^2 + x_1y_1x_2^2z_2^2x_3y_3x_4^2z_4^2P_1P_2(PL_4)^2\ ]\end{aligned}$$

$$\boldsymbol{F} = \mathbf{1} - x_2y_2P_1 - x_4y_4P_2 + x_2y_2x_4y_4P_1P_2, \boldsymbol{G} = x_1\,y_1 - x_1x_4\,y_1y_4P_2$$

$$\begin{aligned}\boldsymbol{H} = j\big(&x_1x_2x_3x_4y_2y_3y_4z_1\,.PL_4PL_8 - x_4^2y_4^2x_1x_2x_3y_2y_3z_1.P_2PL_4PL_8 - x_4^2z_4^2x_1x_2x_3y_2y_3\,z_1.P_2PL_4PL_8\\ &- x_2^2y_2^2x_1x_3x_4y_3y_4z_1.\ P_1PL_4PL_8 + x_2^2x_4^2y_2^2y_4^2x_1x_3y_3z_1.\ P_1P_2PL_4PL_8\\ &+ x_2^2x_4^2y_2^2z_4^2x_1x_3y_3z_1\ P_1P_2.PL_4PL_8 - x_2^2z_2^2x_1x_4x_3y_3y_4z_1\,.P_1PL_4PL_8\\ &+ x_2^2x_4^2z_2^2y_4^2x_1x_3y_3z_1.P_1P_2PL_4PL_8 + x_2^2x_4^2z_2^2z_4^2x_1x_3y_3z_1\,.P_1P_2PL_4PL_8\big)\end{aligned}$$

$$\begin{aligned}\boldsymbol{I} = -\big(&x_1x_3x_4y_4z_1z_3PL_8^2 - x_4^2y_4^2x_1x_3z_1z_3P_2PL_8^2 - x_4^2z_4^2x_1x_3z_1z_3P_2PL_8^2 - x_1x_2x_3x_4z_1z_3y_2y_4P_1PL_8^2\\ &+ x_4^2y_4^2x_1x_2x_3y_2z_1z_3P_1P_2PL_8^2 + x_4^2z_4^2x_1x_2x_3y_2z_1z_3P_1P_2PL_8^2\big)\end{aligned}$$

$$\boldsymbol{J} = \mathbf{1} - x_4y_4P_2, \boldsymbol{K} = x_3y_3(\mathbf{1} - x_2y_2P_1)\,, \boldsymbol{L} = x_2x_3y_2z_3PL_8 - x_2^2y_2^2x_3z_3P_1PL_8 - x_2^2z_2^2x_3z_3P_1PL_8\ ,\ \boldsymbol{M} = (\mathbf{1} - x_2y_2P_1)$$

$$\boldsymbol{S = \left[x_1y_1x_2y_2x_3y_3 - x_1y_1x_2y_2x_3^2y_3^2P_2 - x_1y_1x_2y_2x_2^2z_3^2P_2 - x_1y_1x_2^2y_2^2x\square y_3P_1 + x_1y_1x_2^2y_2^2x_3^2y_3^2P_1P_2 + x_1y_1x_2^2y_2^2x_2\square z_3^2P_1P_2 - x_1y_1x_3y_3x_2^2z_2^2 + x_1y_1x_3^2y_3^2x_2^2z_2^2P_2 + x_1y_1x_2^2z_2^2x_3^2z_3^2P_2\right]PL_8}$$

$T = 1 - x_2y_2P_1 - x_3y_3P_2 + x_2y_2x_3y_3P_1P_2$

$x_1 = \sqrt{1-\gamma_1}\,, \quad y_1 = \sqrt{1-\kappa_1}\,, \quad z_1 = \sqrt{\kappa_1}$

$x_2 = \sqrt{1-\gamma_2}\,, \quad y_2 = \sqrt{1-\kappa_2}\,, \quad z_2 = \sqrt{\kappa_2}$

$x_3 = \sqrt{1-\gamma_3}\,, \quad y_3 = \sqrt{1-\kappa_3}\,, \quad z_3 = \sqrt{\kappa_3}$

$x_4 = \sqrt{1-\gamma_4}\,, \quad y_4 = \sqrt{1-\kappa_4}\,, \quad z_4 = \sqrt{\kappa_4}$

$P_1 = e^{-\frac{\alpha}{2}L_R - jk_nL_R}\,, P_2 = e^{-\frac{\alpha}{2}L_L - jk_nL_L} \;: L_R = 2\pi R_R\,, L_L = 2\pi R_L$

$PL_2 = e^{-\frac{\alpha}{2}L_D - jk_nL_D}\,, PL_4 = e^{-\frac{\alpha L_D}{2\ 2} - jk_n\frac{L_D}{2}}\,, \;\; PL_8 = e^{-\frac{\alpha L_D}{2\ 4} - jk_n\frac{L_D}{4}}$

and

$$E_{th_2} = \left[\frac{G.F^2 - \mathrm{G.F.}C - A.H.J}{F^2.J - C.\mathrm{F.}J}\right]E_{in_2} + \left[\frac{(F.I - B.H - C.I)}{F.(F-C)}\right]E_{ad_3}$$

$$E_{dr_3} = \frac{K(F - C - BL/K)E_{ad_3} - L.A.E_{in_2}}{M(F-C)}$$

$$E_{ad_3} = E_{dr_1}(\sqrt{1-\kappa} - \sqrt{\kappa}^2(\frac{Q}{S-T})$$

$$E_{th_3} = \left[\frac{G.F^2 - \mathrm{G.F.}C - A.H.J}{F^2.J - C.\mathrm{F.}J}\right]E_{in_3} + \left[\frac{(F.I - B.H - C.I)}{F.(F-C)}\right]E_{ad_5}$$

$$E_{dr_5} = \frac{K(F - C - BL/K)E_{ad_5} - L.A.E_{in_3}}{M(F-C)}$$

$$E_{ad_5} = E_{dr_3}(\sqrt{1-\kappa} - \sqrt{\kappa}^2(\frac{Q}{S-T})$$

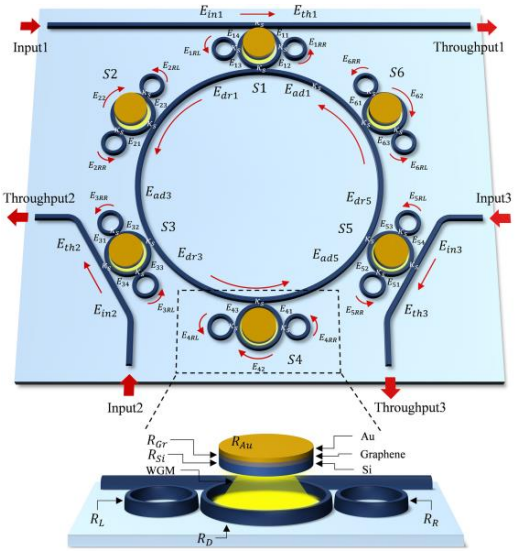

Figure 1: Schematic of a plasmonic island structure, where $\boldsymbol{E_{in}}$, $\boldsymbol{E_{th}}$, $\boldsymbol{E_{dr}}$, $\boldsymbol{E_{ad}}$ are the electrical fields of the input, through, drop and add ports, $\boldsymbol{R_R}$, $\boldsymbol{R_L}$, and $\boldsymbol{R_D}$ are the right, the left, and the centre ring, respectively, κ_s : the coupling coefficients are 0.5. $\boldsymbol{R_{Si}}$: Silicon circle radius, $\boldsymbol{R_{Gr}}$: Graphene circle radius, and $\boldsymbol{R_{Au}}$: Gold sphere radius.

3. Simulation Results

In the simulations, three different wavelengths 1.10, 1.30 and 1.55 μm are input into the system along the propagation axis (z-axis), as shown in Figure 1.Light power is fed into the system and described by the given equations in the previous section. Under the resonant condition, the multiplexed light sources are formed and the output signals are obtained at the islands and through ports. These signals are the multiplexed wavelength outputs within the identified areas, which can be used to form the distributed sensor areas with different wavelengths. This means that various sensors can be used by distributed sensors within the given area. From the preliminary results obtained by the graphical approach, where the selected parameters are given by the related figure captions. The simulation results are obtained by using the MATLAB program. The plot of the WGM outputs of the distributed nodes is shown in Figure 2. The input power of the light source is 45 mW is kept same for three different center wavelengths i.e.,1.30 µm, 1.55 µm, and 1.10 µm and each is fed into the Input1 port, Input 2 port, and Input 3 port, respectively. The ring system, R_L = R_R = 0.5 µm, R_D = 1.0 µm. The coupling constants are κ_1 to κ_4 are the same, which is 0.5. The ring material is the *InGaAsP/InP*, of which the refractive index; n_0= 3.14, n_2= 1.3×10^{-17} m^{2}W^{-1}. Throughput port signals of the system are shown in Figure 3, where the light input power is 15 mW, the variation of the input power results is plotted in Figure 4, where the input power is varied from 10-30 mW. Resulting changes in the spectral widths in terms of the free spectral range (FSR) of the sensor nodes is shown in Figure 5. The graphical approach is used by Optiwave program to acquire optimized parameters The results plotted in Figure 2 are obtained by using these optimized parameters in Matlab based simulations. The same light source is input into the circulator via the input port of three different nodes(Panda-ring resonators). Light power from the different directions and wavelengths are coupled into the selected node and circulated in the optical circulator, in which the output is obtained at the nodes and the through ports. The resonant WGMs are fed and seen at the node centers, which are the reference signals of distributed sensors. The exciting environment related to the change in the free spectrum range to the sensor node will change the device parameters and the refractive indices, which can be measured in term of the change in the wavelength as the reference positions, for an instant, the distributed temperature on the interesting surface and the bio-cell distributed sensors. For the electro-optic conversion of the island nodes, the electron mobility, $\boldsymbol{\mu = \frac{V_d}{E}}$, where $\boldsymbol{V_d}$ is Drift velocity, which is $\boldsymbol{v_d = \frac{j_s}{nq}}$, where $\boldsymbol{j_s = \sigma LE}$ is the current density flowing through the material, L is the material length (thickness), and $\boldsymbol{n}$ is the charge-carrier number density (electrons per cubic meter). The charge-carrier number density, $\boldsymbol{n}$ = [Density×free electron number per atom×Avogadro's constant]/[Molar mass] electrons per cubic meter. For Au, the density is 19.32 gcm^{-3}, the Avogadro's constant is 6.02×10^{23} atoms, the free electron number is 1, the Molar mass is 196.967 gmol^{-1}, and the conductivity, σ = 4.10×10^7 Sm^{-1} [15-17]. By using the parameters are $\boldsymbol{R_{Si} = R_{Gr} = R_{Au}}$ = 800 nm, the thickness of each layer, Si, Graphene, and Gold, is 0.2 µm, 0.1 µm, and 0.1 µm, respectively. The output mobility can be obtained and used for the electrical sensors. The dimension of the device scale and parameters are given within the fabrication

capabilities of available technology [18-20] that can be used as the realistic system for bio-cell sensors[21], where the cell contents may be placed on the system. From which the difference in the shited in the free spectral range will be the measurement.

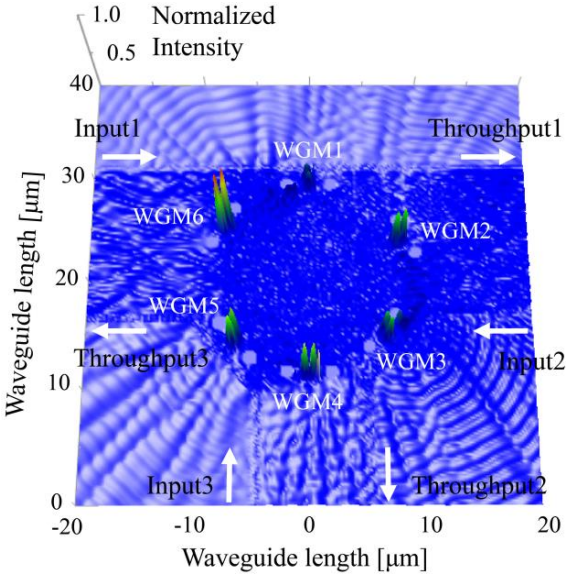

Figure 2: The plot of the WGM outputs of the system in Figure 1, where the input light source power is 45 mW of the three different center wavelengths of 1.10, 1.30 μm, 1.55 μm. The ring system, $\boldsymbol{R_L}$ = $\boldsymbol{R_R}$ = 0.5 μm, $\boldsymbol{R_D}$ = 1.0 μm. All the coupling constants are the same, where $\boldsymbol{\kappa_1}$ to $\boldsymbol{\kappa_4}$ = 0.5. The ring material is the ***InGaAsP/InP***, of which the refractive index; $\boldsymbol{n_0}$= 3.14, $\boldsymbol{n_2}$= 1.3×10^{-17} m^2W^{-1}.

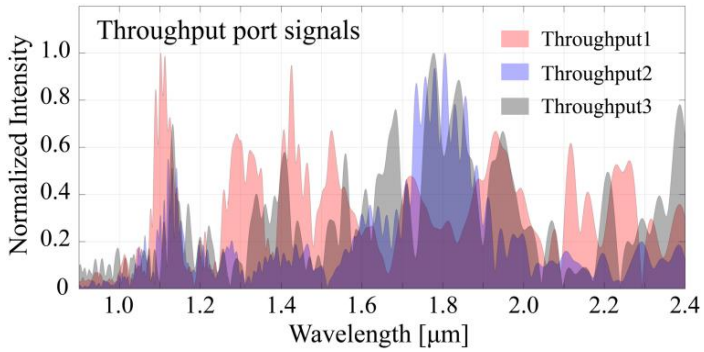

Figure 3: The plots of the throughput port signals of the system in Figure 1, where the light input power is at 15 mW, the waveguide loss is 0.10 dBcm^{-1}, the core effective area is 0.30-0.50 μm^2 .

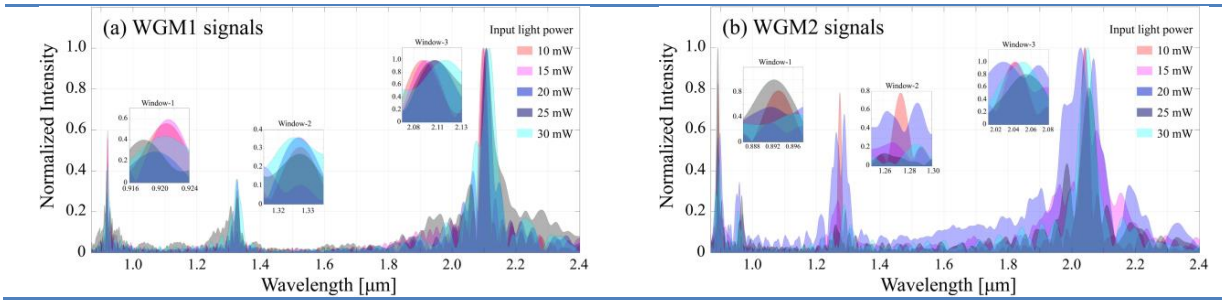

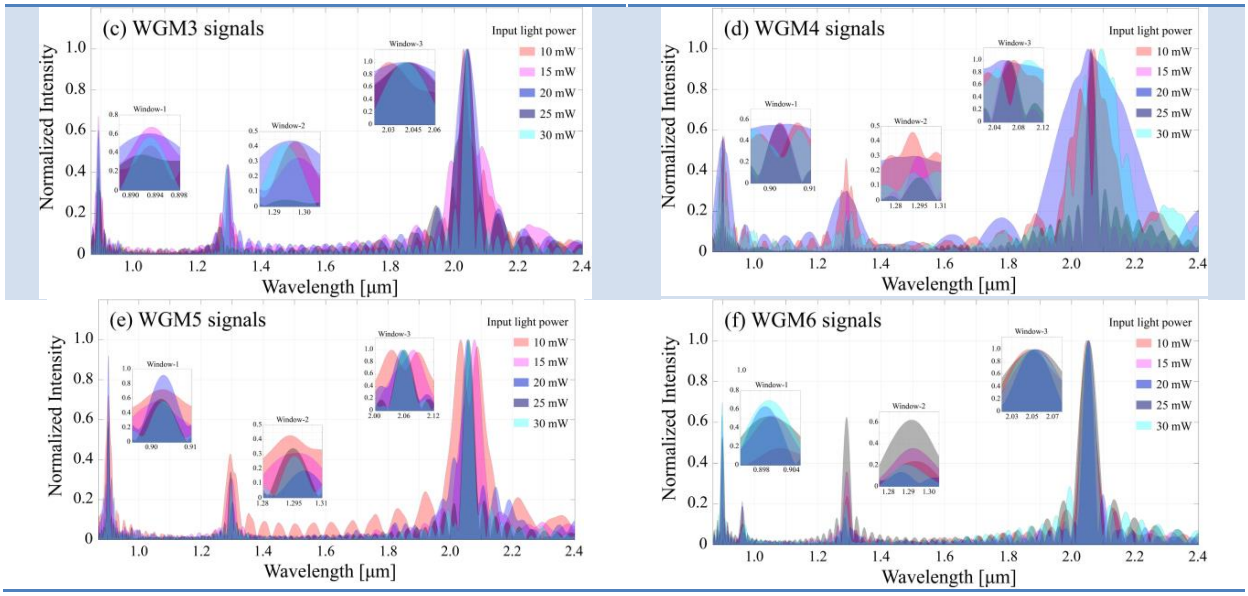

Figure 4: The plots of the changes in the WGM outputs and the input power from 10-30 mW of the sensor nodes(islands). The changes in the center wavelength($\Delta\lambda$) positions are seen. This is the manipulation of the multiwavelength distributed sensors by changing the input power, where (a)-(f) are the results of nodes(WGMs) 1-6.

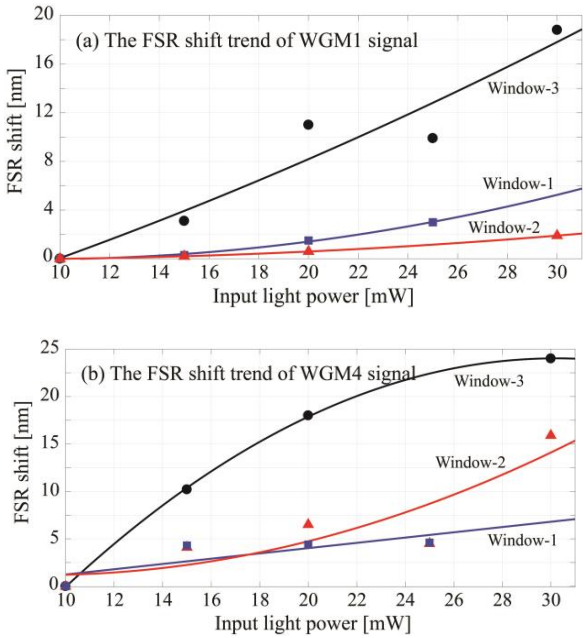

Figure 5: The plots of the changes in the free spectral range($\Delta\lambda$) and the input power of the nodes 1 and 4, in which the trends are the curve fitting plots. It is shown the potential of using as the multiwavelength distributed sensors.

4. Conclusion

The use of a microring resonator system embedded by the plasmonic island to form the distributed sensors is proposed. The simulations have shown the promising results that the relationship between the changes in the free spectrum range and the input power can be configured to be the multiwavelength distributed sensors. The resulting shift in wavelength of the distributed sensors can be a useful measurement for bio-cell sensors. Moreover, the sensor nodes can be increased to have larger distributed areas to expand the coverage area, where the communication among cells in the different nodes can also be possible. The plasmonic island performs the electro-optic conversion, which enables the application of this sensor system for both optical and electrical systems.

Acknowledgment

P. Yupapin would like to acknowledge for the research facilities from Ton Duc Thang University, Vietnam. J. Ali would like to acknowledge the research funding provided by MOHE through FRGS grant (4F891) Universiti Teknologi Malaysia for the research facilities.

References

[1] J. Ali , P. Youplao, N. Pornsuwancharoen et al., “On-chip remote charger model using plasmonic island circuit. Results in Physics, 9: 815-818(2018).
[2] J. Ali, P. Youplao, N. Pornsuwancharoen et al., “On-chip Electro-optic multiplexing circuit using serial microring boxcar filters”, Results in Physics, 10, 18-21(2018).
[3] N. Pornsuwancharoen, P. Youplao, M.S. Aziz et al., “In-situ 3D micro-sensor model using embedded plasmonic island for biosensors,” Microsystem Technologies, 1-5, 2018. Early online.
[4] N. Pornsuwancharoen, P. Youplao, I. Amiri et al., "Electron driven mobility model by light on the stacked metal–dielectric interfaces," Microwave and Optical Technology Letters, 59, 1704-1709(2017).
[5] N. Pornsuwancharoen, I.S. Amiri, F. Suhailin et al., "Micro-current source generated by a WGM of light within a stacked silicon-graphene-Au waveguide," IEEE Photonics Technology Letters, 29, 1768-1771(2017).
[6] S. Punthawanunt, M.S. Aziz, P. Phatharacorn et al., “LiFi Cross-connection node model using whispering gallery mode of light in a microring resonator,” Microsystem Technologies, 1-6, 2018, Online First.
[7] K. Yothapakdee, P. P. Yupapin, and K. Tamee, “Brain signal monitoring model using THz whispering gallery modes generated by micro-conjugate mirror probe,” J. IFSA Sensors and Transducers, 186(3), 112-117(2015).
[8] S.C. Hagness, D. Rafizadeh, S.T. Ho et al., ST, FDTD Microcavity simulations: Design and experimental realization of waveguide-coupled single-mode ring and whispering-gallery-mode disk resonators. IEEE Journal of Lightwave Technology, 15(11), 2145-2165(1997).
[9] J. Ali, N. Pornsuwancharoen, P. Youplao et al., “Coherent light squeezing states within a modified microring system,” Results in Physics, 9, 211-214(2018).
[10] M. Wolverton, “Whispering resonances to the terahertz regime”, Scilight, 2018, 060002 (2018); 10.1063/1.5024669.
[11] D.W. Vogt and R. Leonhardt, “Ultra-high Q terahertz whispering-gallery modes in a silicon resonator”, APL Photonics, 3, 051702 (2018); doi: 10.1063/1.5010364.
[12] P. Phatharacorn, S. Chiangga and P. Yupapin, “Analytical and simulation results of a triple micro whispering gallery mode probe system for a 3D blood flow rate sensor,” Appl. Opt., 55(33), 009504(2016).
[13] P. Phatharacorn, S. Chiangga, J. Ali and P. Yupapin, “Micro-optical probe model using integrated triple microring resonators for vertical depth identification,” Microsystem Technologies, 2018, 1-7, Early online.
[14] P. Youplao, N. Sarapat, N. Pornsuwancharoen et al., “Plasmonic op-amp circuit model using the inline successive microring pumping technique,” Microsystem Technologies, 2018, pp. 1-7. Early online.
[15] S. Soysouvanh, M.A. Jalil, I.S. Amiri et al., “Ultra-fast electro-optic switching control using a soliton pulse within a modified add-drop multiplexer”, Microsystem Technologies 2018, 1-6: Early Online.
[16] K. Chaiwong, K. Tamee, S. Punthawanunt et al., “Naked-eye 3D imaging model using the embedded micro-conjugate mirrors within the medical micro-needle device,” Microsystem Technologies, 24, 2695-2699(2018).
[17] J. Ali, K. Chaiwong, P. Youplao et al., “MIMO multi-channels for simultaneous electro-optic distributed sensors,” Results in Physics, 2018, 1-4, Submitted.
[18] A.H. Atabaki, S. Moazenni, F. Pavanello et al., Integrating photonics with silicon nanoelectronics for next generation of system on a chip. Nature 556, 349-354(2018).
[19] C. Koos, L. Jacome, C. Poulton et al., "Nonlinear silicon-on-insulator waveguides for all-optical signal processing", Optics Express, 15: 5976-5990(2007).
[20] P.J. Mohr, D.B. Newell, B.N. Taylor, “CODATA recommended values of the fundamental physical constants”, Rev. Mod. Phys., 88: 035009-1-73(2016).
[21] P. Youplao, N. Pornsuwancharoen, I.S. Amiri et al., “Microring Stereo Sensor Model using Kerr-Vernier Effect for Bio-Cell Sensor and Communication,” Nanocommunication Networks, 2018, in press.